IOP Conf. Series: Materials Science and Engineering **425** (2018) 012008 doi:10.1088/1757-899X/425/1/012008

Impact of different clearance heights on the operation of a water-flooded twin-screw expander—experimental investigations based on indicator diagrams

A Nikolov[1] **and A Brümmer**[1]

[1]Chair of Fluidics, TU Dortmund University, Dortmund, Germany

E-mail: alexander.nikolov@tu-dortmund.de

Abstract. Twin-screw expanders offer a high potential for energy conversion in the lower and medium power range, for instance in Rankine cycle systems for exhaust heat recovery. With the aim of minimising internal leakages within the expander and lubricating moving machine parts, an auxiliary liquid can be carried with the main flow or liquid working fluid can be fed to the twin-screw expander. Moreover, the operation of twin-screw expanders in Rankine cycle systems at high liquid mass fractions and in trilateral flash cycles is predicted to be a very promising application for expanders in lower power ranges. Thus, a fundamental understanding of the operation of liquid-flooded twin-screw expanders is mandatory. This paper presents results of an experimental investigation into a water-flooded twin-screw expander prototype SE 51.2 designed at the Chair of Fluidics at TU Dortmund University. On the one hand, the aspect of a two-phase working fluid is discussed considering integral characteristic numbers such as mass flow, delivery rate, and effective isentropic efficiency. On the other hand, in order to explain the influence mechanisms of a two-phase working fluid on the operating behaviour of the twin-screw expander, indicator diagrams are recorded by means of high-resolution pressure transmitters to determine indicated power. Hence, mechanical and hydraulic losses, indicated isentropic efficiency, and mechanical efficiency of the twin-screw expander can be calculated. In order to determine the influence of the narrow clearance on the hydraulic losses and the clearance sealing effect in terms of a two-phase working fluid, a systematic variation of the rotor-tip clearance height is carried out. As a result of the investigations, a water surge at the rotor tip is proved to be a significant mechanism affecting hydraulic losses in a water-flooded twin-screw expander.

1. Introduction

Due to the growing shortage of non-renewable fossil fuel reserves and the consequential increase in primary energy costs, underdeveloped energy potentials are increasingly moving into the focus of economic interest. Available heat sources in the field of decentralised energy systems of small and medium power ranges from 3 kW to 1.5 MW [1, 2]—such as industrial exhaust gases or waste heat in vehicle engines, geothermal or solar thermal energy—can be converted into usable mechanical power by means of expanders or turbines within a Rankine cycle system.

In this context, twin-screw expanders in Rankine cycles possess clear advantages compared with turbomachines or even other volumetric expander concepts, being capable of economically transforming small volume flows at relatively large pressure ratios [3]. In general, twin-screw machines are characterised by relatively high energy density and efficiency, advantageous part load behaviour, and a

rather simple design [4]. Furthermore, twin-screw expanders in (organic) Rankine cycles are suitable for wet-vapour operation; thus, an overheating system is not essential [5]. On the one hand, the number of system components and the overall costs can be reduced. On the other hand, liquid in twin-screw expanders could be beneficial with regard to their operation. The auxiliary fluid also reduces noise emissions and thermal stress within the machine parts and seals structurally necessary machine clearances [6].

Investigations into water- and oil-injected twin-screw expanders with timing gears were carried out by Zellermann [7]. Kauder and Zellermann [8] reported a significant increase of hydraulic friction losses in terms of oil-injection at high rotor tip-speeds. Hence, the operating range of wet-running screw machines taking hydraulic losses into account is usually restricted to a maximum rotor tip-speed of 40 $m \cdot s^{-1}$ [4]. Without limitations in the rotor tip-speed, performance reduction due to oil shearing in and at the machine clearances exceeds the positive sealing effect of the injected liquid. In this context, Harling [6] has carried out extensive experimental studies on the distribution of the injected oil in a twin-screw compressor, considering the oil-surge theory of Kauder [9]. Here, losses as a result of momentum exchange between the oil and the rotor surface have been investigated. In order to determine hydraulic friction losses in screw expander clearances using an auxiliary liquid, an analytical approach was presented by Gräßer and Brümmer with regard to water [10] and oil [11, 12]. In [13], Vasuthevan and Brümmer proved by means of numerical simulations that hydraulic losses generated by a water surge at the rotor-tip are more significant compared to water friction within the rotor-tip clearance. In [14], the operational behaviour of a small oil-flooded twin-screw expander in an organic Rankine cycle system has been experimentally and theoretically investigated. Kliem [15] examined a twin-screw expander application in a trilateral flash cycle theoretically and experimentally. Here, overheated water is injected into the working chamber where it expands and evaporates. According to Ohman and Lundqvist [1], this application of twin-screw expanders is predicted to be a promising approach in the medium and low power operating range. In this context, a method for the theoretical investigation into twin-screw expanders in trilateral flash cycles has been presented by Vasuthevan and Brümmer [16]. With regard to thermal deformation, Svigler *et al.* [17] reported that under water-injected conditions, the thermal deformation of the rotor flank in twin-screw compressors corresponds to the manufacturing tolerance magnitude for ground rotors.

Hereinafter, the results obtained from pursuing experimental investigations into the operation of a water-flooded twin-screw expander based on the studies presented in [18] and [19] are discussed. In [18], the effect of water-flooded operation has been presented integrally from an energetic point of view considering effective isentropic efficiency and delivery rate of the test expander. At part load operation and at low rotor tip-speeds in particular, it has been demonstrated that the water-flooded compared to the dry-running twin-screw expander reveals higher effective isentropic efficiency. At high rotor tip-speeds however, expander efficiency declines with increasing amounts of water, since hydraulic losses become more dominant. In [19], indicator diagrams were presented in order to quantify mechanical power losses in the twin-screw expander and to identity the main influence physical mechanisms with respect to water-flooded operation. Generally, mechanical power losses in twin-screw expanders can be attributed to friction losses in the grease-lubricated bearings and in the rotor contact as well as to acceleration of the auxiliary fluid and hydraulic friction in the clearances and in the water surge at the rotor tips. Within the framework of the following study, a methodical variation of the rotor-tip clearance height is carried out in order to detect its impact on hydraulic losses and clearance sealing in terms of water in the working chamber.

2. Experimental setup

A detailed description of the experimental setup within the framework of the investigations has been presented in [18] and [19]. A 3D model of the test twin-screw expander prototype SE 51.2 and the positions of the high-resolution pressure indication transmitters are illustrated in figure 1. SE 51.2 is a twin-screw expander prototype without timing gears. The transmission of torque occurs directly via contact between the rotor flanks. The screw rotors are hardened and have a tough tungsten

carbide/carbon (WC/C) wear-protection coating, so seizure can be avoided in dry-running or water-flooded operation. Both fixed and loose bearing sets are grease lubricated, so no oil supply is necessary. Details about the expander geometry parameters are listed in table 1. For the purposes of the experimental investigations, the rotor-tip clearance height has been varied in order to analyse how hydraulic losses change and which are the consequences on the reduction of internal leakages in the expander. The clearance height variation has been achieved by increasing the rotor bore diameter keeping any further expander geometry parameters constant.

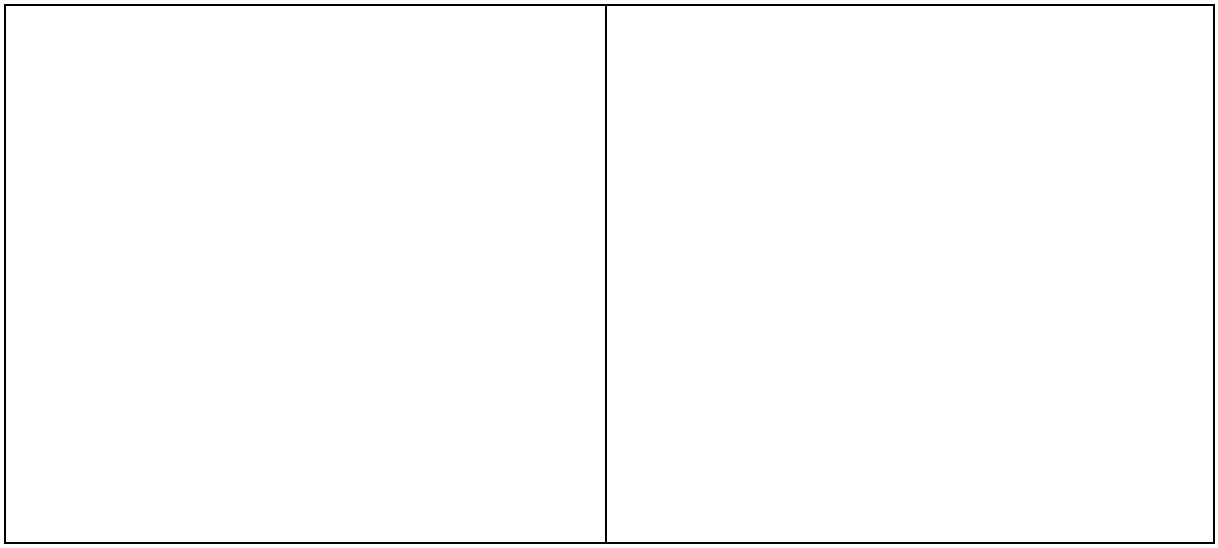

Figure 1. Positions of pressure indication transmitters (0…6), inlet and outlet area, as well as volume curve of the test screw expander SE 51.2 including ranges of male rotor rotational angle corresponding to each pressure transmitter.

Table 1. Parameters of the test screw expander SE 51.2.

designation	**unit**	**male rotor (MR)**	**female rotor (FR)**
number of lobes z	[-]	3	5
diameter d	[mm]	71.8	67.5
rotor lead s	[mm]	181.8	303
wrap angle φ	[°]	200	-120
rotor length l	[mm]	101	
rotor profile	[-]	modified asymmetric SRM	
axis-centre distance a	[mm]	51.2	
internal volume ratio v_i	[-]	2.5	
displaced volume per male rotor rotation V	[cm^3]	286	
front clearance height $h_{fc,hp}$ (high pressure)	[mm]	0.1	
front clearance height $h_{fc,lp}$ (low pressure)	[mm]	0.17	
rotor-tip (housing) clearance height h_{hc}	[mm]	0.08, 0.16, 0.24	

The relevant measurement devices installed in the test rig and the twin-screw expander are listed in table 2. To record the indicator diagrams of the test twin-screw expander, two different piezoresistive sensor types are installed flush with the rotor bore surface and on the high-pressure front side. The pressure transducers of the series M5 manufactured by “KELLER AG für Druckmesstechnik” at position 0, 1, and 6 record the absolute static pressure in the inlet port (position 0), in the working

chamber in the range of rotational angle between 85° and 130° (position 1), and during the fluid discharge on the low-pressure side of the expander (position 6). With regard to the manufacturer data sheet, a natural frequency of more than 50 kHz can be expected. At positions 2 to 5, XTM-190 pressure transducers manufactured by "Kulite Semiconductor Products, Inc" with natural frequency higher than 425 kHz are installed. Hence, no acoustic or vibration issues at the pressure metering point with regard to eigenfrequencies are expected. Depending on pressure and temperature, the sensitivity of each XTM-190 sensor was calibrated in order to increase its accuracy. Due to a relatively high temperature related zero point offset of the XTM-190 sensors, only the relative change in pressure to a reference pressure level is considered. For this reason, the pressure difference between two adjacent transducers within their overlapping scope (figure 1) is set to zero and the high-resolution static pressure at position 6 is used as a starting reference pressure level.

Table 2. Measuring range and accuracy of installed measurement devices.

parameter	**range**	**accuracy**	**type (manufacturer)**
chamber pressure p	0 to $10 \cdot 10^5$ Pa (absolute)	±0.2 % FS* (linearity)	series M5 (KELLER AG für Druckmesstechnik)
chamber pressure p	0 to $17 \cdot 10^5$ Pa (absolute)	$\pm 10^3$ Pa (linearity calibrated)	XTM-190 (Kulite Semiconductor Products, Inc.)
inlet pressure p_i	0 to $6 \cdot 10^5$ Pa (relative)	±0.1 % FS*	ATM.1ST (STS)
temperature ϑ	-185…300 °C	±1 °C (-40…133 °C)	insulated thermocouples type T
torque M_{MR}	±20 Nm	±0.1 % FS*	ETH DRLF-II-n (ETH-messtechnik)
rotational speed n_{MR}	max. 19,000 min^{-1}	-	
air mass flow $\dot{m}_a$	max. ≈ 3300 $kg \cdot h^{-1}$ (at $p_i = 5.5 \cdot 10^5$ Pa)	±0.35 % o.r.**	Promass 83F (DN40) (Endress+Hauser)
water volume flow	max. 8.2 $l \cdot min^{-1}$	±(0.4 % o.r.** + 0.02 % FS*)	ProcessMaster300 (ABB)

*FS–full scale; **o.r.–of reading

With regard to the pressure indication, a rotational angle range between 130° and 140° cannot be covered due to lack of space in the casing, so the pressure has to be estimated. Preliminary analysis of the recorded pressure revealed that a linear pressure distribution in the missing range is qualitatively and quantitatively sufficiently accurate. At low rotor speeds, the pressure transmitter at position 0 is assumed to represent the chamber pressure from the beginning of the working cycle at rotational angle of 45° up to rotational angle of 85° as indicated in figure 1. In this way, the assumed chamber pressure is mapped with regard to an ideal chamber filling without pressure drop over the inlet. In theory, this results in an upper limit for the converted work within this working cycle range. At higher rotational speeds, a different approach to map the chamber pressure profile in this section is applied. Here, linear pressure increase starting from the outlet and ending at the pressure level of the transmitter at position 1 is assumed. This method is more appropriate with respect to increasing inlet throttling losses at higher rotor speeds or increasing amount of injected water. Therefore, the pressure level and the indicated work within the missing range of the indicator diagram are expected to be lower than the real one during the chamber growth. This approach represents a lower limit for the indicated work within the first 40° of chamber development the range of rotational angle between 45° and 85°.

Within the framework of this experimental investigation, both the system and the twin-screw expander operating parameters were varied. Water was injected into the high-pressure domain at a superficial water temperature of $\vartheta_{i,w} \approx 60$ °C at constant air inlet pressures of $p_i = 3 \cdot 10^5$ Pa, $p_i = 4 \cdot 10^5$ Pa, $p_i = 5 \cdot 10^5$ Pa as well as superficial air temperature of $\vartheta_{i,a} = 90$ °C. Outlet pressure

corresponds to ambient conditions at ca. $p_o \approx 1 \cdot 10^5$ Pa. The resulting mixture temperature at the expander inlet is nearly $\vartheta_i \approx 50$ °C depending on water volume flow and expander rotational speed.

In the style of steam or vapour mass fraction, the amount of injected water into the expander inlet port is represented by the dryness fraction x relating air mass flow to the overall air and water mass flow:

$$x = \frac{\dot{m}_a}{\dot{m}_a + \dot{m}_w}. \tag{1}$$

Here, measured air mass flow $\dot{m}_a$ (Coriolis mass flow meter) can be considered as dry air, since a refrigerant type dryer is used after air compression. Water volume flow is recorded by means of an electromagnetic flow-metering device. Regarding water temperature to ambient conditions, water density and mass flow $\dot{m}_w$ can be determined. Dryness fraction of $x = 1$ corresponds to a dry-running operation and $0 < x < 1$ to the two-phase flow in water-flooded operation. Dryness fraction x is varied in the range between 1.0 and 0.4. For water injection, two nozzle sizes are used at two adjacent water flow ranges with respect to a satisfactorily homogeneous water injection quality in the expander inlet domain. The maximum expander rotational speed is n_{MR} = 18,000 min^{-1} which equals a male rotor tip-speed of u_{MR} = 67.7 m·s^{-1}.

3. Characteristic numbers

Using characteristic numbers, physical processes or the operation of machines can be quantitatively analysed and compared with each other. In the following analysis, different characteristic numbers are used to explain the relevant effects on the operation of the test twin-screw expander.

3.1. Delivery rate

Delivery rate λ_L is a characteristic number that quantifies mass loss mechanisms such as internal or external leakages, throttling losses during the chamber filling, or thermal effects within a displacement machine. Taking the actual measured air mass flow $\dot{m}_a$ and the theoretical air mass flow $\dot{m}_{th}$ of the twin-screw expander into account, delivery rate is defined as:

$$\lambda_L = \frac{\dot{m}_a}{\dot{m}_{th}}. \tag{2}$$

Here, the theoretical mass flow $\dot{m}_{th}$ is referred to dry-air density $\rho_{da,i}$ in the inlet domain taking the chamber volume at the begin of the internal expansion $V_{th,ex}$ (chamber volume at male rotor rotational angle of 201° in figure 1), the male rotor speed n_{MR}, and the number of the male rotor lobes z_{MR} into account:

$$\dot{m}_{th} = \rho_{da,i} \cdot V_{th,ex} \cdot n_{MR} \cdot z_{MR}. \tag{3}$$

The chamber volume displaced by liquid can be ignored due to a relatively high volume fraction of air. As already mentioned in [19], considering a homogeneous two-phase mixture in the working chamber, air volume fraction is more than 98.5 % even at the lowest air mass flow and highest water flow. Thus, $V_{th,ex}$ refers to the working chamber volume after completing the chamber filling. Furthermore, dry air is considered as an ideal gas and its density $\rho_{da,i}$ is determined by means of the calculated subcooled temperature after water was injected. In terms of delivery rate, measured air mass flow $\dot{m}_a$ does not consider evaporated water steam with respect to saturated humid air after water injection, since the Coriolis mass flow meter is installed upstream of the water injection nozzle. In some cases, at high temperature levels and low pressure at the same time, steam fraction has to be taken into account, since it significantly increases. Within the following investigations, steam mass flow increases to a level of

up to 3.2 % of metered air mass flow at the lowest inlet pressure and dryness fraction. Since steam mass flow is not measured by the Coriolis flow meter, an additional decrease of delivery rate (section 3.1) of a maximum of 3.2 % may arise at some operating points.

3.2. Indicated and effective isentropic efficiency

Indicated and effective isentropic efficiency ($\eta_{i,s}$ and $\eta_{e,s}$) reveal the energetic potential of the twin-screw expander considering different loss mechanisms. Here, indicated or effective power is related to the isentropic potential of the working fluid considering the inlet and outlet conditions. With respect to water-flooded operation, an isentropic change in state represents the maximum energy available in the two-phase working fluid. Hence, indicated isentropic efficiency is defined as:

$$\eta_{i,s} = \frac{P_i}{\Delta \dot{H}_s} \tag{4}$$

and effective isentropic efficiency respectively as:

$$\eta_{e,s} = \frac{P_e}{\Delta \dot{H}_s}. \tag{5}$$

Indicated power P_i can be calculated by means of the time-dependent working chamber pressure p and volume V, male rotor rotational speed n_{MR}, and number of male rotor lobes z_{MR} as follows:

$$P_i = -n_{MR} \cdot z_{MR} \cdot \oint p \cdot dV. \tag{6}$$

Effective power P_e results from the recorded male rotor rotational speed n_{MR} and torque M_{MR} as:

$$P_e = 2 \cdot \pi \cdot n_{MR} \cdot M_{MR}. \tag{7}$$

Isentropic enthalpy flow $\Delta \dot{H}_s$ for a homogeneous mixture is defined as the product of dry-air mass flow $\dot{m}_{da}$ and the specific isentropic enthalpy difference for humid air $\Delta h_{1+x,s}$ between expander outlet (o) and inlet (i) as follows:

$$\Delta \dot{H}_s = \dot{m}_{da} \cdot \Delta h_{1+x,s} = \dot{m}_{da} \cdot \left(h_{1+x,s,o} - h_{1+x,i}\right). \tag{8}$$

In this context, the specific enthalpy h_{1+x} for a homogeneous humid-air-water mixture in thermodynamic equilibrium can be calculated with reference to water load X [20]. Water load X represents the ratio of water mass flow $\dot{m}_w$ to dry-air mass flow $\dot{m}_{da}$:

$$X = \frac{\dot{m}_w}{\dot{m}_{da}}. \tag{9}$$

Since water load of the pressurised and preheated air at expander inlet upstream of water injection is negligibly low, dry-air mass flow $\dot{m}_{da}$ can be related to measured air mass flow $\dot{m}_a$. The specific enthalpy of unsaturated humid air ($X < X_{sat}$) is defined as:

$$h_{1+x} = c_{p,da} \cdot \vartheta + X \cdot \left(r_w + c_{p,ws} \cdot \vartheta\right). \tag{10}$$

Here, water load X_{sat} corresponds to humid air at a relative humidity of 100 %. The specific enthalpy of saturated humid air ($X \geq X_{sat}$) with reference to water in the mixture can be calculated as:

$$h_{1+x} = c_{p,da} \cdot \vartheta + X_{sat} \cdot \left(r_w + c_{p,ws} \cdot \vartheta\right) + (X - X_{sat}) \cdot c_w \cdot \vartheta. \quad (11)$$

For temperatures $\vartheta < 0$ °C, the calculation of the specific humid air enthalpy is referred to ice condensation as follows:

$$h_{1+x} = c_{p,da} \cdot \vartheta + X_{sat} \cdot \left(r_w + c_{p,ws} \cdot \vartheta\right) - (X - X_{sat}) \cdot (r_{ice} - c_{ice} \cdot \vartheta). \quad (12)$$

The constant fluid properties required to calculate the enthalpy of the humid-air-water mixture are listed in table 3. Specific enthalpy of humid air at the expander inlet can be calculated by means of the recorded inlet temperature ϑ_i and pressure p_i. Isentropic fluid mixture temperature and enthalpy at the expander outlet is calculated with regard to a constant specific entropy at the expander inlet and outlet according to [20].

Table 3. Constant fluid properties for the fluid state calculation of humid air in thermodynamic equilibrium [20].

designation	**unit**	**value**
dry-air heat capacity $c_{p,da}$	[J·kg^{-1}·K^{-1}]	1004.6
water-steam heat capacity $c_{p,ws}$	[J·kg^{-1}·K^{-1}]	1863
liquid water heat capacity c_w	[J·kg^{-1}·K^{-1}]	4185
triple temperature ϑ_{tr}	[°C]	0.01
ice heat capacity c_{ice} at ϑ_{tr}	[J·kg^{-1}·K^{-1}]	2070
specific solidification enthalpy r_{ice} at ϑ_{tr}	[kJ·kg^{-1}]	333.4
specific vaporisation enthalpy r_w at ϑ_{tr}	[kJ·kg^{-1}]	2500.9

3.3. Mechanical efficiency

Mechanical efficiency η_m is a characteristic number that quantifies mechanical power losses in twin-screw expanders relating effective and indicated power to each other:

$$\eta_m = \frac{P_e}{P_i}. \quad (13)$$

In the twin-screw expander investigated, mechanical power losses result from the contact between both screw rotors, within the bearings and sealing elements, as well as from hydraulic losses considering acceleration and hydraulic friction of the injected auxiliary fluid in and at the clearances and rotor surfaces. Mechanical power loss $\dot{\Phi}$ can be calculated as follows:

$$\dot{\Phi} = P_i - P_e. \quad (14)$$

Hence, mechanical efficiency of the twin-screw expander can be calculated as:

$$\eta_m = \frac{P_e}{P_i} = \frac{P_i - \dot{\Phi}}{P_i} = 1 - \frac{\dot{\Phi}}{P_i}. \quad (15)$$

By means of equation (4) and equation (5), mechanical efficiency η_m can be also determined from the ratio of effective isentropic to indicated isentropic efficiency as:

$$\eta_m = \frac{\eta_{e,s}}{\eta_{i,s}}. \tag{16}$$

4. Results

In this section, results from the experimental investigations into the water-flooded twin-screw expander considering effects of rotor-tip clearance height variation are presented. First, indicator diagrams are discussed revealing the impact of different clearance situations on the working chamber pressure during a working cycle under dry-running and water-flooded conditions. After that, expander operating maps based on characteristic numbers are used to quantify the arguments discussed initially.

4.1. Indicator diagrams

Recording the chamber pressure during a working cycle and generating indicator diagrams is a common method to evaluate the available fluid energy within the working chamber of a reciprocating machine and respectively of a twin-screw expander. In this way, indicated power takes throttling losses, leakages, under- and overexpansion, as well as the interaction between the working and auxiliary fluid and the working chamber boundaries into account. Moreover, the different influence mechanisms can be quantitatively illustrated by variation of the expander operation parameters.

In order to illustrate the influence of water on the chamber pressure at different rotor-tip clearance heights, indicator diagrams at a high and a low male rotor tip-speed are presented in figure 2 and figure 3. Each operating point corresponds to a constant inlet pressure and superficial air and water temperatures. Generally, at both rotor tip-speed levels, water in the working chamber mostly initiates an increase in chamber pressure during internal expansion and a greater indicated power respectively (except for rotor-tip clearance height of 0.08 mm in figure 3). As explained in [19], this effect can be primarily traced back to the extensive heat exchange between water and the expanding gaseous fluid, so the polytropic expansion exponent is reduced compared to a pure gaseous operation. Additionally, a sealing effect resulting from water in the clearances is expected, while this can be only partially proved by means of the indicator diagrams.

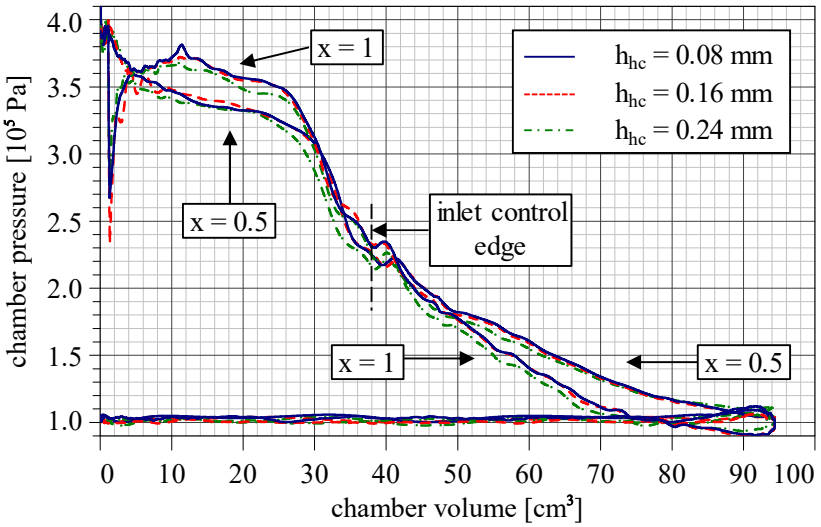

Figure 2. Indicator diagrams at a male rotor tip-speed of 67.7 m·s^{-1}, an inlet pressure of 4·10^5 Pa, a superficial air temperature of 90 °C, and a superficial water temperature of 60 °C; *dryness fraction: 1 and 0.5; rotor-tip clearance height: 0.08 mm, 0.16 mm, and 0.24 mm.*

Generally, at high rotor tip-speeds, the internal leakages related to the expander air mass flow can be neglected, so no significant impact of clearance height on the indicator diagrams is expected. In fact, inlet throttling and hydraulic losses become dominant. In figure 2, a significant drop in pressure during the chamber filling can be observed under water-flooded conditions due to increasing inlet throttling. The main reason for the pressure increase during the internal expansion at high rotor tip-speeds is the heat flow from the liquid phase into the gaseous fluid. Hence, overexpansion can be avoided. In a rotor-related coordinate system considering the clearance sealing effect, it is more likely to have a boundary-driven (Couette) water back-flow from the leading chamber as a consequence of a relative motion between the rotor tip and the housing boundary. The pressure-driven (Poiseuille) water flow plays a subordinate role and merely reduces the Couette water flow from the leading chamber. At lower dryness fractions, a liquid surge is expected to form at the rotor-tip clearance outlet on the leading chamber side. On the one hand, this would reduce the clearance cross-section for the gaseous flow and seal the clearance (which is in fact not a dominant effect at higher rotor tip-speeds). Clearance sealing in terms of water-flooded operation is discussed in section 4.2 using delivery rate as defined in equation (2). On the other hand, hydraulic losses become dominant. In section 4.3, hydraulic friction losses resulting from liquid friction in the clearances and in the water surge at the rotor tip in the leading working chamber are analysed by means of mechanical power loss and mechanical efficiency.

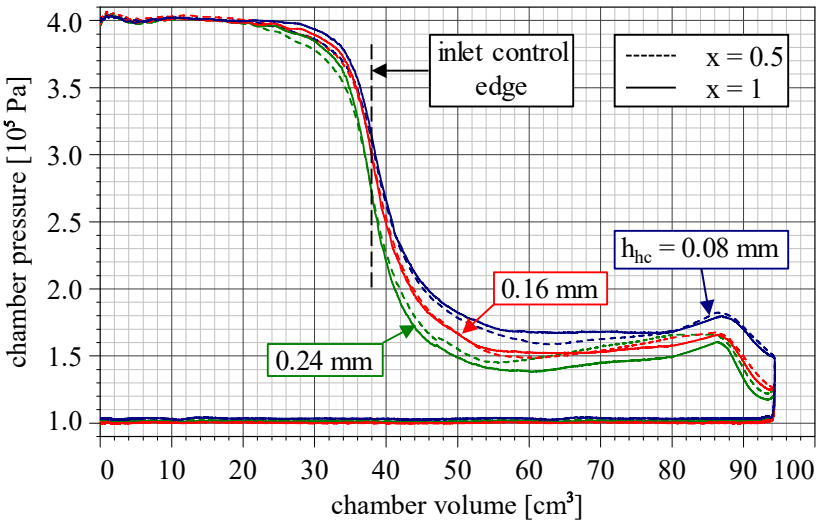

Figure 3. Indicator diagrams at a male rotor tip-speed of 3.8 $m \cdot s^{-1}$, an inlet pressure of $4 \cdot 10^5$ Pa, a superficial air temperature of 90 °C, and a superficial water temperature of 60 °C; *dryness fraction: 1 and 0.5; rotor-tip clearance height: 0.08 mm, 0.16 mm, and 0.24 mm*.

In contrast, at low rotor tip-speeds, internal leakage becomes more relevant, while the influence of inlet throttling declines or disappears as illustrated in figure 3. Due to internal leakage, higher pressure is revealed in the working chamber during the internal expansion unlike at high rotor tip-speed in figure 2. A chamber refilling is the result. In terms of inlet throttling, no significant pressure drop as a function of clearance height and only a minor influence of dryness fraction on chamber filling are observed. Under water-flooded conditions, expander operation leads to less significant boundary-driven (Couette) water flow in the clearances, so now the pressure-driven (Poiseuille) water flow predominates. For different clearance heights and approximately comparable pressure difference at the rotor tip, the pressure-driven water clearance volume flow toward the leading chamber increases for greater clearance cross-sections. Therefore, less water might remain at the clearance inlet to effectively seal the clearance. In this context, at a clearance height of 0.08 mm in figure 3, the clearance sealing in the water-flooded expander is relatively effective and overshadows the heat exchange effect. Thus, the pressure in the

chamber declines under the levels seen in dry-running operation. At a clearance height of 0.16 mm, a slight decrease in sealing effect can be observed, since the pressure-driven (Poiseuille) water volume flow in the rotor-tip clearance increases. Moreover, heat exchange in the leading chamber intensifies due to the increased amount of water. Eventually, the lowest sealing effect can be detected at a clearance height of 0.24 mm, resulting in the greatest air and water mass and, thus, enthalpy flow into the leading chamber under water-flooded conditions. Here, a chamber pressure increase can be detected compared to dry-running operation due to a maximum amount of water and heat flow from water to air respectively in the expanding working chamber.

4.2. Mass flow and delivery rate

In figure 4, expander air mass flow and delivery rate are illustrated as functions of the male rotor tip-speed at different dryness fractions. As expected, expander air mass flow increases at higher rotor tip-speeds under dry-running and water-flooded conditions. Reducing dryness fraction, expander air mass flow declines due to reduced internal leakages, increased heat flow from water into air, or greater inlet throttling losses depending on the rotor tip-speed. Since, according to [18], the inlet temperature of the two-phase mixture depends on the amount of water, lower dryness fraction results in higher inlet temperatures and lower air inlet density, since heat flux from water into the gaseous working fluid increases. As a consequence, expander air mass flow may decline depending on dryness fraction, too. To quantify the sealing and inlet throttling effects, delivery rate is considered. At a fixed low rotor tip-speed, a significant drop in delivery rate as a consequence of declining dryness fraction and, hence, increasing clearance sealing effect, can be perceived. In contrast, at a constant high rotor tip-speed, delivery rate drops mainly due to increasing inlet throttling in terms of water-flooded operation as demonstrated in figure 2. As mentioned in section 3.1, an additional decrease in air mass flow and delivery rate due to water steam in the saturated gaseous phase of the two-phase mixture results from water-flooded operation. Nevertheless, at the lowest dryness fraction considered, air mass flow decreases not more than 3.2 % at the lowest and 2.2 % at the highest inlet pressure investigated. Therefore, this effect is neglected within the framework of this study.

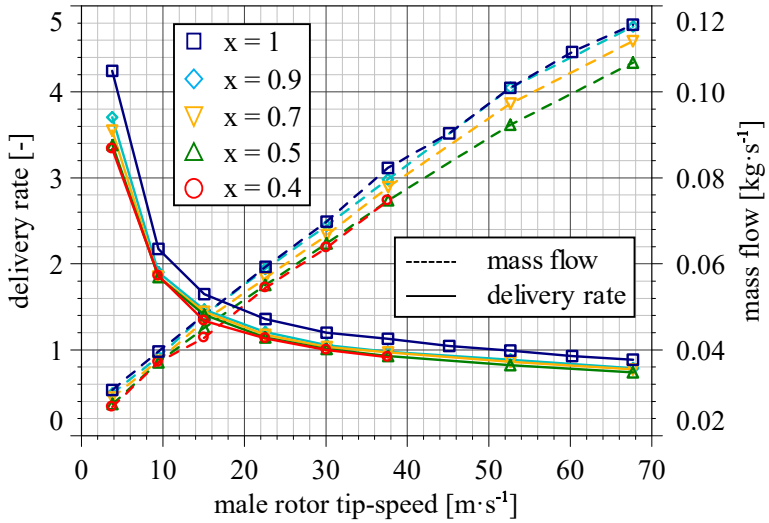

Figure 4. Expander air mass flow and delivery rate depending on male rotor tip-speed at an inlet pressure of $4 \cdot 10^5$ Pa, a superficial air temperature of 90 °C, a superficial water temperature of 60 °C, and a rotor-tip clearance height of 0.08 mm; *dryness fraction: 1, 0.9, 0.7, 0.5, and 0.4*.

In figure 5, the impact of different rotor-tip clearance heights on the expander air mass flow and delivery rate is presented for a constant dryness fraction of 0.5. At low rotor tip-speeds and increasing clearance height, the sealing effect decreases due to increasing pressure-driven (Poiseuille) water volume flow in the high-pressure rotor-tip clearances, so expander air mass flow and delivery rate increase. Up to a rotor tip-speed of about 35 $m \cdot s^{-1}$, the sealing effect of the middle (0.16 mm) compared to the lowest (0.08 mm) clearance height increases continuously according to expander air mass flow and delivery rate. Then, sealing becomes maximum as expander air mass flow and delivery rate at both clearance heights are identical. As explained in section 4.1, this fact can be traced back to the boundary-driven (Couette) water flow providing more liquid to seal the clearance cross-section at rising rotor tip-speed. As a result of the larger clearance cross-section at a clearance height of 0.24 mm in relation to 0.08 mm and 0.16 mm, the sealing effect appears to be relatively inefficient.

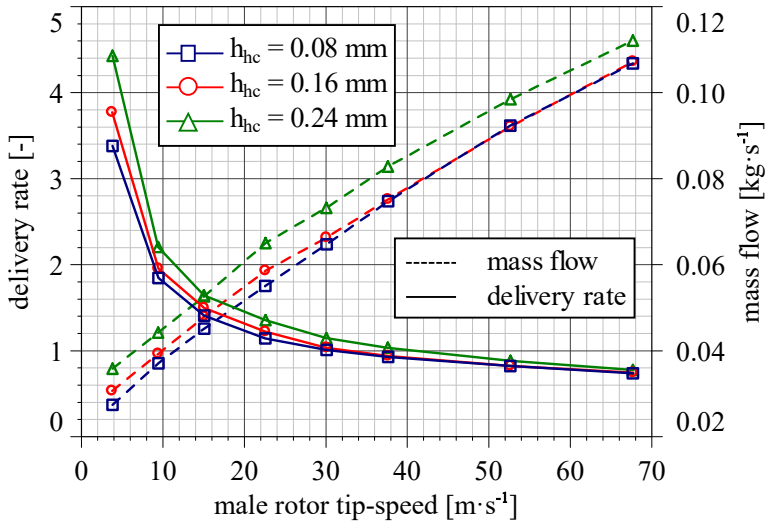

Figure 5. Expander air mass flow and delivery rate at a male rotor tip-speed of 67.7 $m \cdot s^{-1}$, an inlet pressure of $4 \cdot 10^5$ Pa, a superficial air temperature of 90 °C, a superficial water temperature of 60 °C, and a dryness fraction of 0.5; *rotor-tip clearance height: 0.08 mm, 0.16 mm, and 0.24 mm*.

4.3. Mechanical power loss and expander efficiency

Hereinafter, to analyse the influence mechanisms on the operation of the test twin-screw expander from energetic point of view, mechanical power loss and mechanical efficiency respectively as well as indicated and effective isentropic efficiency are considered. Mechanical power loss and different efficiencies depending on rotor tip-speed and clearance height under dry-running and water-flooded conditions are illustrated in figure 6. For dry-running and water-flooded operation, mechanical power loss increases exponentially as a function of male rotor tip-speed. At a dryness fraction of 1, frictional losses in the bearings and in the rotor contact account for the entire mechanical power loss. Under water-flooded conditions, hydraulic shear stress in the narrow clearances and in the water surge at the rotor tip contribute additionally to the overall mechanical power loss. Within the framework of the experimental investigation, mechanical power losses with regard to the water flow in the clearances and the water surge can only be considered integrally. Here, compared to dry-running operation, mechanical power losses in terms of a water-flooded expander significantly increase at each rotor-tip clearance height.

In this context, hydraulic losses at the rotor tip develop differently depending on the rotor position and the applied pressure difference between two adjacent working chambers. On the one hand, during the chamber filling, a pressure-driven (Poiseuille) water flow from the high-pressure to the expanding

working chamber inhibits the forming of a water surge considering low rotor tip-speeds, so hydraulic losses can be avoided. Moreover, the Poiseuille water flow drives the rotor by transferring momentum to the rotor tip and contributes to the expander power, since both pressure-driven water flow and rotor-tip motion work in the same direction. Increasing rotor tip-speed results in higher boundary-driven (Couette) against the pressure-driven (Poiseuille) water flow. As a consequence, the effect of the Poiseuille water flow declines, clearance water flow stagnates, and a water surge starts forming at the rotor tip in the leading working chamber after the Couette water flow rate becomes higher than the pressure-driven flow. At this turning point, the water surge at the high-pressure rotor-tip clearances might reveal a maximum size. A further increase in rotor tip-speed provides higher boundary-driven (Couette) water flow from the leading into the following chamber, so the water surge size declines. On the other hand, at low pressure levels during a working cycle, boundary-driven (Couette) water flow dominates especially at high rotor tip-speeds. In terms of under-expansion at low rotor tip-speeds, a pressure-driven (Poiseuille) flow reduces the boundary-driven (Couette) water flow, which initiates an increase in the water surge size. Nevertheless, the absolute hydraulic loss is relatively low due to lower rotor tip-speed. In this context, hydraulic friction in the clearances and with respect to the water surge have been analysed separately by means of theoretical investigations in [12] and [13]. In [13], hydraulic losses generated by the water surge at the rotor tip are proved to be more significant compared to water friction within the rotor-tip clearances.

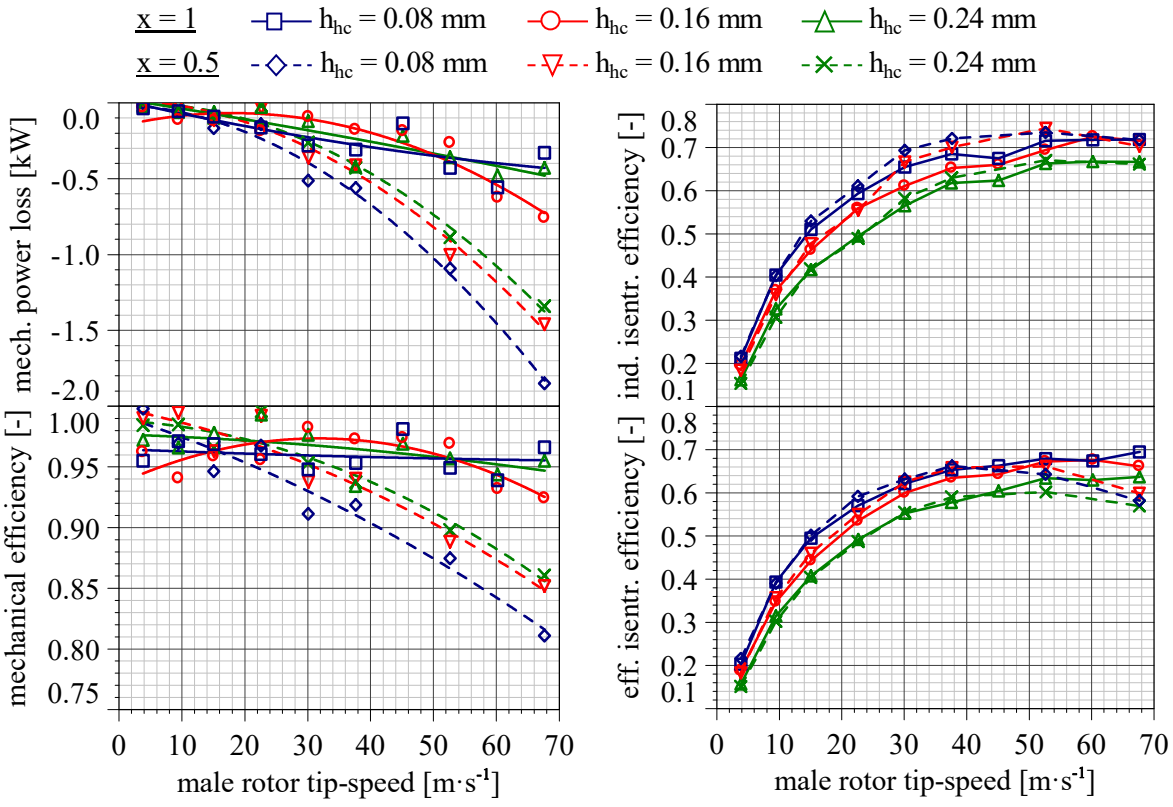

Figure 6. Mechanical power loss, mechanical efficiency, indicated isentropic efficiency, and effective isentropic efficiency depending on male rotor tip-speed at an inlet pressure of $4 \cdot 10^5$ Pa, a superficial air temperature of 90 °C, and a superficial water temperature of 60 °C; *dryness fraction: 1 and 0.5; rotor-tip clearance height: 0.08 mm, 0.16 mm, and 0.24 mm*.

With regard to increasing rotor-tip clearance height in figure 6, mechanical power losses under water-flooded conditions decline significantly, since the boundary-driven Couette water volume flow increases

in relation to the clearance cross-section, so less water remains at the rotor-tip in the leading chamber and the water surge declines or disappears completely. At the same time, hydraulic shear stress within the narrow rotor-tip clearances declines due to increased clearance height that additionally contributes to less friction at the low-pressure clearances or less drive momentum at the clearances corresponding to higher pressure levels. Due to the smaller dimensions of the high-pressure compared to the low-pressure rotor-tip clearances, hydraulic losses due to water surge might significantly overshadow the drive effect in terms of a Poiseuille water flow at the high-pressure rotor-tip clearances.

Relating mechanical power losses to the available energy potential of the fluid in the working chamber, no substantial change in mechanical efficiency due to the lack of hydraulic losses at dry-running operation can be observed as a function of rotor tip-speed (figure 6). Considering a two-phase working fluid at low rotor tip-speeds, no significant influence of water on mechanical efficiency compared to dry-running operation can be detected, either. In contrast, at constant dryness fraction of 0.5, mechanical efficiency declines at increasing rotor tip-speed in consequence of rising hydraulic losses as explained before. Greater rotor-tip clearance heights reveal higher mechanical efficiency levels due to declining size of the water surge and reduced liquid shear stress in the rotor-tip clearances.

In order to quantify different loss mechanisms relative to the available two-phase working fluid potential of the twin-screw expander in figure 6, indicated and effective isentropic efficiency are presented. Considering indicated isentropic efficiency at rising male rotor tip-speed, increases can be identified under dry-running and water-flooded conditions due to the reduced influence of clearance flows on expander operation. Moreover, under-expansion is reduced and the expander operation approaches the design operation conditions when chamber pressure at the end of the expansion equals the discharge pressure. At highest rotor tip-speeds in dry-running operation, indicated isentropic efficiency declines as a consequence of overexpansion and increasing inlet throttling losses. An exception is seen for a rotor-tip clearance height of 0.24 mm where the indicated isentropic efficiency remains relatively constant for dry-running and water-flooded operation due to the slightly lower overexpansion, as presented in figure 2, resulting from the highest internal leakages.

Comparing dry-running and water-flooded operation with each other, basically higher indicated isentropic efficiency at a dryness fraction of 0.5 can be detected due to heat transfer from water into the gaseous working fluid as well as reduced internal leakages with regard to different ranges of rotor tip-speed. The lowest clearance height of 0.08 mm reveals higher indicated isentropic efficiency in the rotor tip-speed range between 10 $m \cdot s^{-1}$ and 60 $m \cdot s^{-1}$, whereas at the greatest clearance height efficiency increases for rotor tip-speeds from 30 $m \cdot s^{-1}$ to 50 $m \cdot s^{-1}$ in water-flooded operation. At the maximum rotor tip-speed, similar indicated isentropic efficiencies are disclosed for both operational modes, since relatively high inlet throttling at a dryness fraction of 0.5 eliminates the advantages of water in the working chamber. In contrast, at lower rotor tip-speed, efficiency even declines as result of relatively high energetic losses in terms of internal leakages. Considering increasing rotor-tip clearance height, indicated isentropic efficiency declines at each dryness fraction considered. This can be again traced back to the increase in internal leakage, expander air mass flow, and delivery rate as presented in section 4.2.

Despite increasing mechanical efficiency at greater rotor-tip clearance heights, a conclusive estimation of the energy conversion made by means of effective isentropic efficiency reveals, as expected, a less advantageous operation under both dry-running and water-flooded conditions. Nevertheless, at constant low clearance height, an increase in effective isentropic efficiency up to male rotor tip-speed of ca. 40 $m \cdot s^{-1}$ to 45 $m \cdot s^{-1}$ can be detected considering a two-phase working fluid. In general, this covers the part load operational range of the test twin-screw expander. Under overload operational conditions, lower effective isentropic efficiencies are determined in a water-flooded compared to a dry-running expander.

Since the interaction between the pressure-driven (Poiseuille) and boundary-driven (Couette) water clearance flow appears to have a significant impact on the development of hydraulic losses as a function of rotor tip-speed, mechanical power loss and different expander efficiencies at three inlet pressure levels are presented in order to prove this fact, figure 7. Here, for dry-running operation, no significant

dependency of mechanical power loss on inlet pressure can be observed. Considering a constant dryness fraction of 0.5, increasing mechanical power loss is unveiled at higher inlet pressure levels. Hence, the pressure level in the working chamber might have a relatively strong impact on the development of the hydraulic losses and the water surge in particular.

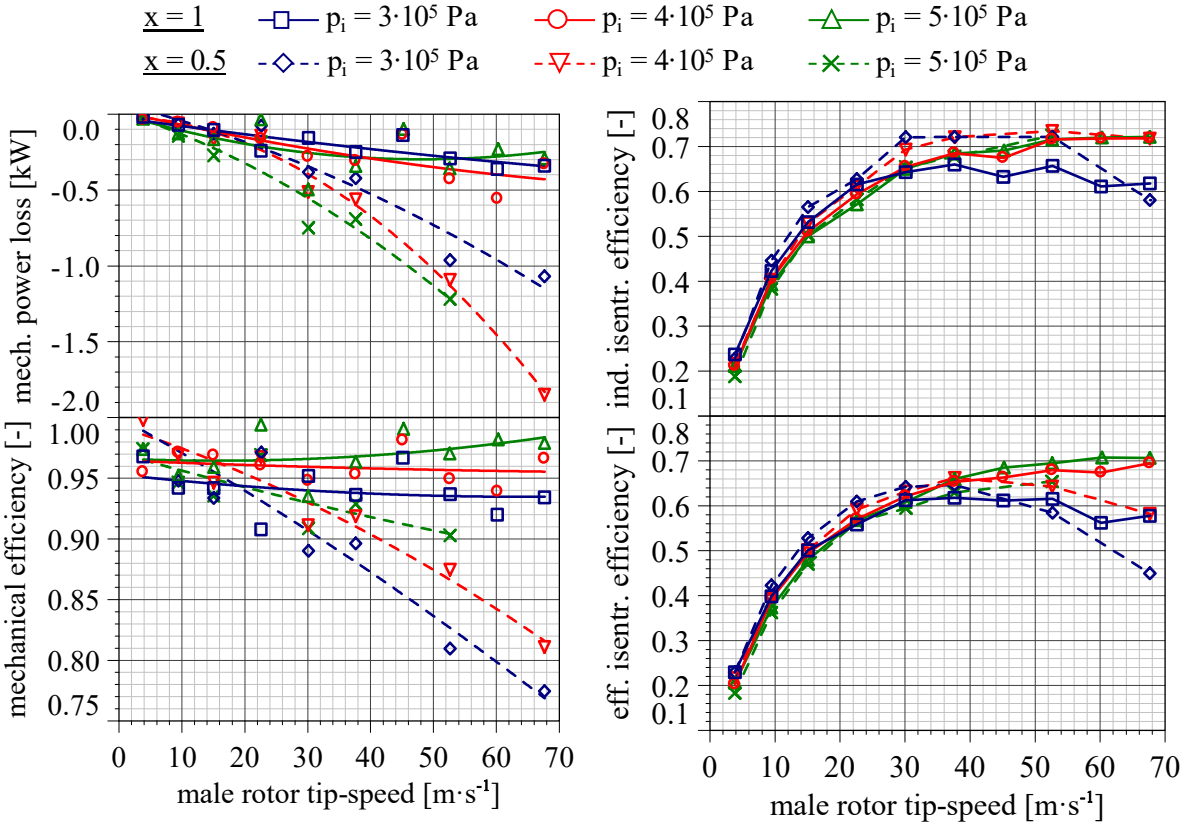

Figure 7. Mechanical power loss, mechanical efficiency, indicated isentropic efficiency, and effective isentropic efficiency depending on male rotor tip-speed at a superficial air temperature of 90 °C, a superficial water temperature of 60 °C, and a rotor-tip clearance height of 0.08 mm; *dryness fraction: 1 and 0.5; inlet pressure: 3·10^5 Pa, 4·10^5 Pa, and 5·10^5 Pa.*

Additional analysis of mechanical power loss depending on injected water volume flow and amount of water in the working chamber respectively at different inlet pressures and rotor-tip clearance heights are presented in figure 8. Here, increasing inlet pressure at rotor-tip clearance height of 0.08 mm unveils a significant rise in mechanical power losses even at lower rotor tip-speeds. In contrast, considering a rotor-tip clearance height of 0.24 mm, this dependency mostly disappears except at the highest rotor tip-speed presented. Since the expander has a fixed internal volume ratio, higher inlet pressure results in increasing pressure difference and Poiseuille water flow at the rotor-tips. The consequence is increasing water surge size at the low-pressure rotor-tip clearances due to a blocking effect of the Poiseuille flow. At the high-pressure rotor-tip clearances, the water surge might decline or disappear at increasing pressure levels, since a greater pressure difference and higher pressure-driven (Poiseuille) water volume flow respectively is present inhibiting the water surge development. Hydraulic shear stress in the narrow rotor-tip clearances at increasing inlet pressure might play a subdominant role compared to the impact of the water surge. Nevertheless, at higher rotor tip-speeds, less shear-stress induced hydraulic losses at the low-pressure rotor-tip clearances due to stagnating water flow could be expected. At the same time at low rotor tip-speeds, drive momentum transferred from the water clearance flow to the high-pressure rotor tips might increase. Bellow the line, as explained before, mechanical power losses under

water-flooded operation increase, since the impact of low-pressure clearances with regard to water surge development overshadows the effect of the Poiseuille flow at high-pressure rotor-tip clearances due to greater clearance width and cross-section respectively.

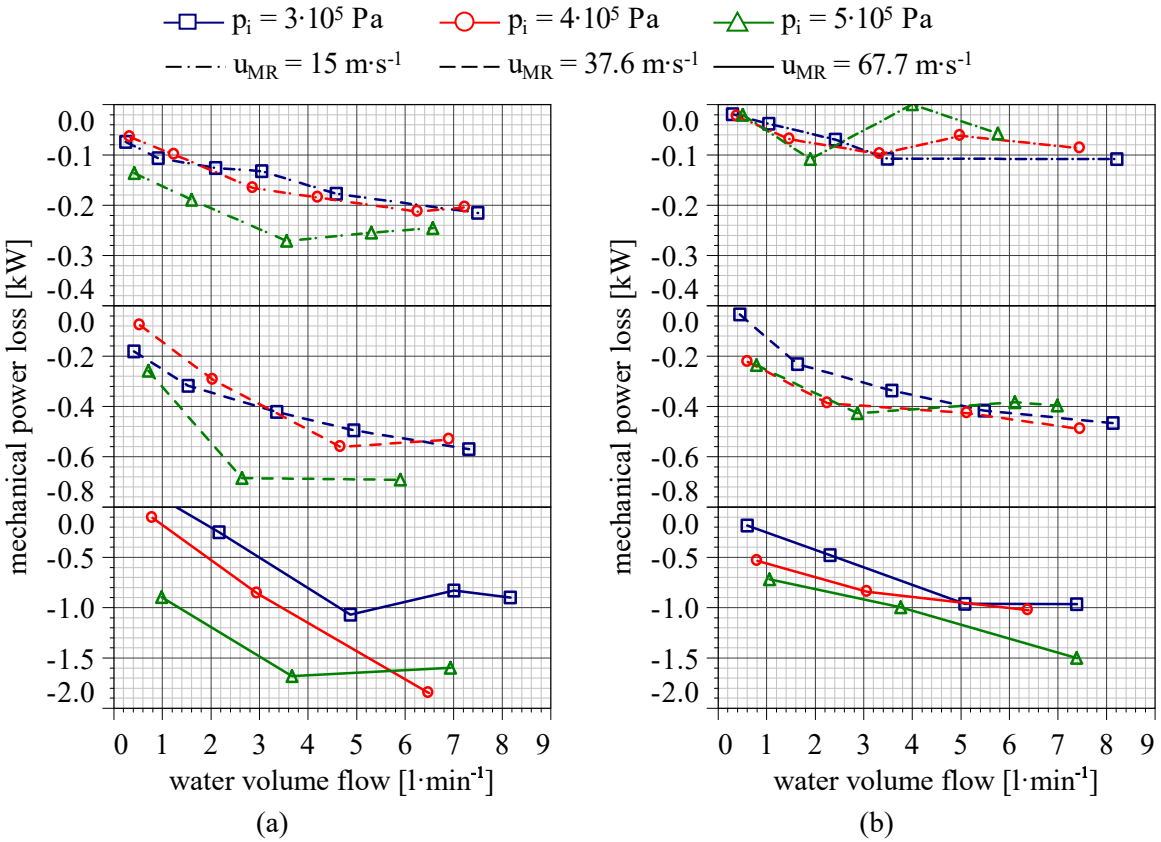

Figure 8. Mechanical power loss as a function of water volume flow at a superficial air temperature of 90 °C and a superficial water temperature of 60 °C; *inlet pressure: $3{\cdot}10^5$ Pa, $4{\cdot}10^5$ Pa, and $5{\cdot}10^5$ Pa; rotor tip-speed: 15 m·s^{-1}, 37.6 m·s^{-1}, and 67.7 m·s^{-1}; rotor-tip clearance height: 0.08 mm (a) and 0.24 mm (b).*

For dry-running operation, no significant dependency of mechanical efficiency on rotor tip-speed can be detected at each inlet pressure presented in figure 7. Under water-flooded conditions, mechanical efficiency decreases at higher rotor tip-speed as discussed before according to figure 6. At constant rotor tip-speed, in contrast to mechanical power loss, mechanical efficiency increases at higher inlet pressure levels under both dry-running and water-flooded conditions. This can generally be traced back to the simultaneously increasing indicated power at higher inlet pressures that even compensates the increase in mechanical power losses under water-flooded conditions. Therefore, at constant rotor tip-speed and water-flooded operation, maximum mechanical efficiency is detected basically at an inlet pressure of $5{\cdot}10^5$ Pa despite maximum mechanical power losses.

In terms of indicated and effective isentropic efficiency at increasing inlet pressure in figure 7, the maximum values generally move to higher rotor tip-speeds for both dryness fractions presented. At constant internal volume ratio, this can be explained, on the one hand, by a greater rotor tip-speed according to transition from under to overexpansion and internal leakages. On the other hand, at high rotor tip-speeds, overexpansion in terms of inlet throttling declines at higher inlet pressure.

Comparing dry-running to water-flooded operation at the maximum inlet pressure of $5{\cdot}10^5$ Pa, a relatively constant indicated isentropic efficiency can be determined. In terms of a two-phase working

fluid, the increasing chamber pressure due to heat flow from water into the gaseous working fluid can explain this fact. Thus, a greater under-expansion at constant expander internal volume ratio is the consequence. Moreover, at low rotor tip-speeds, this effect is additionally sustained by a relatively high pressure-driven (Poiseuille) water volume flow and, hence, less effective clearance sealing. Considering effective isentropic efficiency under water-flooded conditions, lower values compared to dry-running operation result from rising hydraulic losses at higher rotor tip-speeds.

In contrast, a significant increase in indicated isentropic efficiency at an inlet pressure of $3 \cdot 10^5$ Pa is achieved under water-flooded conditions related to dry-running operation. As opposed to the operation at an inlet pressure of $5 \cdot 10^5$ Pa, a more effective clearance sealing due to lower clearance pressure difference and lower pressure-driven (Poiseuille) water flow corresponds to higher efficiency values. At maximum rotor tip-speed, increased overexpansion according to greater inlet throttling reduces the efficiency. Considering effective isentropic efficiency, the sealing effect at low rotor tip-speeds dominates in terms of a two-phase working fluid. At the same time at high rotor tip-speeds, relatively low mechanical efficiency account for declining effective isentropic efficiency.

5. Conclusion and outlook

This paper presents the results of experimental investigations into a water-flooded twin-screw expander with varying operational parameters considering three different rotor-tip clearance heights. This work shows, that the clearance height has a relevant impact on the expander operation in terms of clearance sealing effect and hydraulic losses. In this context, two significant mechanisms were identified—a boundary-driven (Couette) and a pressure-driven (Poiseuille) water clearance flow which, depending on the operational parameters, impact the level of clearance sealing and hydraulic loss induction. Hence, greater rotor-tip clearance height results in lower hydraulic friction losses and higher mechanical efficiencies due to declining shear stress in the clearance and water surge size at the rotor tip. At the same time, analysis of mechanical losses at different inlet pressures and rotor-tip clearance heights have evidenced the significant effect of water surge on the operation of the water-flooded twin-screw expander. Even though a greater rotor-tip clearance height provides an increase in mechanical efficiency, indicated and effective isentropic efficiency reveal worse energy conversion considering both dry-running and water-flooded operation. Finally, the advantages of water-flooded twin-screw expander were identified at part load operation, whereas at higher rotor tip-speeds and overload operation, hydraulic losses significantly affect the effective isentropic efficiency.

In future works, the effect of each twin-screw expander clearance type—rotor-tip clearance, front clearance, interlobe clearance, and blow hole in particular—should be clarified. A further goal is to quantify the determined influence mechanisms by means of characteristic numbers in order to generate a characteristic map of liquid-flooded twin-screw expanders.

References

[1] Ohman H and Lundqvist P 2015 SCREW EXPANDERS IN ORC APPLICATIONS, REVIEW AND A NEW PERSPECTIVE *3rd International Seminar on ORC Power Systems (Brussels, Belgium, 12-14 October)* ed ASME ORC 2015
[2] Hütker J 2016 Energiewandlung in trockenlaufenden Schraubenmotoren *PhD thesis* TU Dortmund University
[3] Kauder K (ed) 1993 *Schraubenmaschinen Nr. 1: Betriebssicherheit und Steuerungen von Schraubenmaschinen (Schraubenmaschinen* Nr. 1*)* (Dortmund: Univ., FG Fluidenergiemaschinen)
[4] Rinder L 1979 *Schraubenverdichter* (Wien, New York: Springer-Verlag)
[5] Brümmer A 2012 Energy efficiency – waste heat utilisation with screw expanders *Prozesstechnik und Komponenten* 120–6
[6] Harling H-B 1994 Untersuchungen zur Ölverteilung in Schraubenkompressoren mit Schmiermitteleinspritzung *PhD thesis* TU Dortmund University

[7] Zellermann R 1996 Optimierung von Schraubenmotoren mit Flüssigkeitseinspritzung *PhD thesis* TU Dortmund University
[8] Kauder K and Zellermann R 1994 Einspritzflüssigkeiten im Schraubenmotor *Schraubenmaschinen '94: Schraubenkompressoren, Schraubenlader, Schraubenmotoren; Tagung Dortmund, 5. und 6. Oktober 1994 (VDI-Berichte* vol 1135*)* ed VDI (Düsseldorf: VDI-Verlag) pp 153–74
[9] Kauder K 1987 Das Öl im Schraubenkompressor - ein Faktor für optimale Betriebsverhaeltnisse *Pumpen Vakuumpumpen Kompressoren, Nürnberg: Harnisch* 38–44
[10] Gräßer M and Brümmer A 2014 An analytic model of the incompressible one-phase clearance flow in liquid injected screw expanders *International Conference on Screw Machines 2014 (TU Dortmund University, Germany, 23rd-24th September) (VDI-Berichte* vol 2228*)* (Düsseldorf: VDI-Verl.) pp 71–89
[11] Gräßer M and Brümmer A 2015 Influence of liquid in clearances on the operational behaviour of twin screw expanders *IOP Conference Series: Materials Science and Engineering* **90** 12060
[12] Gräßer M and Brümmer A 2016 Influence of water and oil clearance flow on the operational behavior of screw expanders *Proceedings of the Institution of Mechanical Engineers, Part E: Journal of Process Mechanical Engineering* **231** 38–46
[13] Vasuthevan H and Brümmer A 2018 Multiphase-flow simulation of a rotating rectangular profile within a cylinder in terms of hydraulic loss mechanisms *International Conference on Screw Machines (TU Dortmund University, Germany, 18th-19th September)* ed IoP
[14] Nikolov A and Brümmer A 2017 Investigating a Small Oil-Flooded Twin-Screw Expander for Waste-Heat Utilisation in Organic Rankine Cycle Systems *Energies* **10** 869
[15] Kliem B 2005 Grundlagen des Zweiphasen-Schraubenmotors *PhD thesis* TU Dortmund University
[16] Vasuthevan H and Brümmer A 2016 Thermodynamic Modeling of Screw Expander in a Trilateral Flash Cycle *23rd International Compressor Engineering Conference at Purdue: West Lafayette, Indiana, USA, 11-14 July 2016 (Purdue)* ed Purdue University Libraries
[17] Svigler J, Rinder L, Rehounek L and Kuchler M 2005 Temperaturdeformation der Rotoren bei nass laufenden Schraubenkompressoren *Schraubenmaschinen: KaSim, Simulationen, Temperaturdeformationen, Energiewandler in BHKW´s, GASSCREW, SCREW (Schraubenmaschinen)* ed K Kauder pp 17–36
[18] Nikolov A and Brümmer A 2014 Influence of water injection on the operating behaviour of screw expanders: Experimental investigation *International Conference on Screw Machines 2014 (TU Dortmund University, Germany, 23rd-24th September) (VDI-Berichte* vol 2228*)* (Düsseldorf: VDI-Verl.) pp 43–60
[19] Nikolov A and Brümmer A 2016 Analysis of Indicator Diagrams of a Water Injected Twin-shaft Screw-type Expander *23rd International Compressor Engineering Conference at Purdue: West Lafayette, Indiana, USA, 11-14 July 2016 (Purdue)* ed Purdue University Libraries
[20] Baehr H D and Kabelac S 2012 *Thermodynamik: Grundlagen und technische Anwendungen (Springer-Lehrbuch)* 15th edn (Berlin u.a.: Springer Vieweg)